Science of the Total Environment 1001 (2025) 180578

Contents lists available at ScienceDirect

Science of the Total Environment

journal homepage: www.elsevier.com/locate/scitotenv

Insights into the 100 largest European surface ozone episodes during spring–summer 2003–2022

Tahimy Fuentes-Alvarez [a,*], Carlos Ordóñez [a], Ricardo García-Herrera [a,b], David Barriopedro [b], Rodrigo Crespo-Miguel [a], Miguel M. Lima [c]

[a] Departamento de Física de la Tierra y Astrofísica, Facultad de Ciencias Físicas, Universidad Complutense de Madrid, Madrid, Spain
[b] Instituto de Geociencias (IGEO), Consejo Superior de Investigaciones Científicas-Universidad Complutense de Madrid (CSIC-UCM), Madrid, Spain
[c] Instituto Dom Luiz, Faculty of Sciences, University of Lisbon, Lisbon, Portugal

HIGHLIGHTS

- Ozone episodes cluster in northern (southern/central) Europe during spring (summer)
- Episodes linked to distinct synoptic conditions depending on the region
- Importance of high-pressure systems and wildfire emissions in eastern Europe
- Differing flow patterns and low precursor concentrations in the British Isles
- High-pressures in western/central Europe and enhanced subsidence in the south

GRAPHICAL ABSTRACT

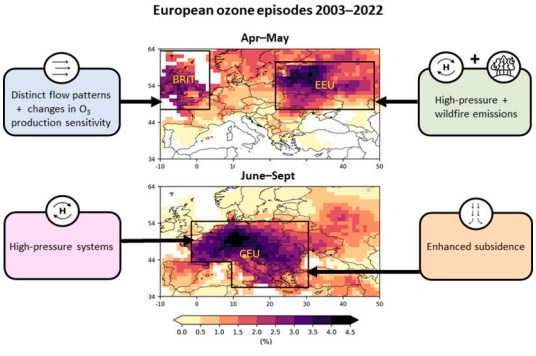

ARTICLE INFO

Keywords:
Surface ozone
Air pollution
Air quality
Synoptic meteorology
Wildfire emissions

ABSTRACT

In this study, we investigate the spatial distribution and drivers of the 100 largest ozone episodes identified in the Copernicus Atmosphere Monitoring Service global reanalysis over Europe during April–September 2003–2022. Using a semi-Lagrangian algorithm to detect large-scale ozone episodes and an atmospheric blocking and subtropical ridge identification method, we analyse the role of meteorological processes and precursor emissions in three key regions: the British Isles (BRIT) and Eastern Europe (EEU) during April–May, and Central Europe (CEU) in June–September, revealing some regional differences. The 28 days with ozone episodes in EEU are associated with anticyclonic conditions but also require elevated concentrations of precursors, often linked to wildfire activity. In contrast, episodes affecting BRIT are characterized by negative anomalies of 500 hPa geopotential height and daily maximum temperature at 2 m as well as stronger than usual winds that ventilate the region. Out of a total of 38 days with episode there, one-quarter are associated with easterly flow and changes in ozone formation sensitivity and three-quarters present varying dynamical conditions. In CEU, we identify significant north-south differences: while 36 out of a total of 60 days with episodes in northern CEU are strongly influenced by blocks and ridges, the 29 days with episodes restricted to the south are affected by weaker synoptic forcing and enhanced subsidence. These findings are relevant for future air quality assessments as they demonstrate that

* Corresponding author.
E-mail address: tahifuen@ucm.es (T. Fuentes-Alvarez).

https://doi.org/10.1016/j.scitotenv.2025.180578
Received 17 July 2025; Received in revised form 5 September 2025; Accepted 19 September 2025
Available online 23 September 2025

the occurrence of large-scale ozone episodes in Europe is driven by region-specific combinations of meteorological conditions and precursor availability.

1. Introduction

Tropospheric ozone (O_3) is a secondary air pollutant formed through complex photochemical reactions involving precursors such as nitrogen oxides ($NO_x = NO_2 + NO$), non-methane volatile organic compounds (NMVOCs), carbon monoxide (CO), and methane (CH_4) in the presence of sunlight. Another source is the injection of O_3 from the stratosphere, while dry deposition to the Earth's surface and chemical loss provide the main sinks (Atkinson, 2000; Monks et al., 2015). Ozone can persist in the polluted boundary layer for a few hours to days, whereas in the free troposphere its lifetime extends to weeks, allowing regional transport (Monks et al., 2015). This pollutant has detrimental effects on humans and vegetation. High levels of O_3 close to the surface pose serious threats to human health, increasing mortality risk and exacerbating respiratory and cardiovascular diseases (GBD 2019 Risk Factors Collaborators, 2020). The negative effects on vegetation lead to reduced agricultural yields and forest productivity (Booker et al., 2009).

Several studies have examined the relationship between near-surface ozone levels and meteorological conditions at northern mid-latitudes during spring and summer (e.g., (Bloomfield et al., 1996; Seo et al., 2014; Otero et al., 2016). While this relationship is complex and nonlinear, it is well established that surface ozone concentrations are highly dependent on solar radiation, temperature, cloud cover and the dilution capacity of the atmosphere. The highest concentrations often occur under high temperatures, stagnant conditions and peak solar radiation, which enhance photochemical production and the accumulation of both O_3 and its precursors (Jacob and Winner, 2009; Otero et al., 2016, and references therein).

Over the last years, a number of studies have addressed the connection between tropospheric ozone and circulation patterns in Europe. Some of them have established the role of the atmospheric circulation in controlling the short and long-range transport of ozone, its formation, destruction and the interactions with precursors (Demuzere et al., 2009; Doche et al., 2014; Zanis et al., 2014; Carro-Calvo et al., 2017). These works have highlighted the contribution of horizontal advection of warm and dry air (Demuzere et al., 2009; Carro-Calvo et al., 2017) and the downward transport from the upper troposphere (Doche et al., 2014; Zanis et al., 2014) to elevated O_3 concentrations in the lower troposphere. Other analyses have investigated the role of high-pressure systems, such as blocks and subtropical ridges. Atmospheric blocks are persistent high-pressure systems that interrupt the prevailing westerly winds at middle and high latitudes, whereas subtropical ridges are temporary poleward intrusions of the subtropical belt into mid-latitudes (Sousa et al., 2018, 2021). The meteorological conditions associated with blocks and ridges, namely subsidence, high temperatures, reduced precipitation, and weak winds in the core of the anticyclone, are conducive to high surface ozone concentrations (Ordóñez et al., 2017; Otero et al., 2022). These authors applied different methods to detect high-pressure systems in the mid-troposphere and investigate their association with elevated ozone. Ordóñez et al. (2017) used two separate algorithms to identify high-latitude blocks and subtropical ridges (Sousa et al., 2017, 2018). They reported that European blocking events significantly increase ozone concentrations, with anomalies of 5–10 ppb across large areas of Europe during spring and summer, while subtropical ridges contribute to enhanced ozone levels over the centre and south of the continent, especially in summer. The influence of blocking on surface ozone in central and eastern Europe was documented by Otero et al. (2022) using a two-dimensional blocking index (Scherrer et al., 2006). Their findings indicate that blocking can increase the probability of the joint occurrence of extreme ozone and temperature events by more than 35 %.

As the meteorological mechanisms contributing to high near-surface ozone levels may vary from one region to another, some studies have applied different types of cluster analyses to identify regions or groups of stations that exhibit consistent spatiotemporal patterns (Lyapina et al., 2016; Carro-Calvo et al., 2017; Boleti et al., 2020). More recently, Crespo-Miguel et al. (2024), henceforth CM2024, have developed a semi-Lagrangian algorithm for the identification and tracking of large-scale ozone episodes in gridded datasets. The algorithm identifies ozone extremes as exceedances of the local 95th percentiles of daily ozone maxima, which are first merged into daily patterns and then into ozone episodes if they are connected in space and time. Overall, an ozone episode is detected if daily patterns (i.e., spatially connected daily ozone exceedances) with a minimum areal extent of 250,000 km^2 persist for three or more days, with an overlap of at least 50 % between consecutive days. For more details, including specific conditions under which these criteria are relaxed, the reader is referred to the original study by CM2024. The algorithm was applied to daily ozone maxima over Europe from the CAMS global reanalysis (EAC4) during April–September 2003–2022, identifying a total of 974 episodes with durations ranging from 3 to 30 days and integrated areal extents from 25,000 to 46,000,000 km^2. They reported that the centres of around one third of the 100 largest episodes (in terms of integrated areal extent) were located north of 50° N during April–May (AM) while the remaining two thirds of the episodes had their centres south of 50° N between June and September (JJAS) (see Fig. 4 of that paper). However, their study did not provide a detailed description of the regions affected by those episodes and only addressed the role of the meteorological conditions for the top ten episodes.

The main aim of this work is to understand the spatiotemporal patterns and drivers of major ozone episode in Europe during the spring and summer months. To do so, episodes must be characterized as part of large structures rather than as isolated phenomena. For that purpose, we build on the results by CM2024 and investigate the 100 largest European ozone episodes in the CAMS reanalysis during April–September 2003–2022, with integrated extensions during their life cycles ranging from 1,900,000 to 46,000,000 km^2. We conduct separate analyses to identify the main affected regions during the periods mentioned above, i.e. AM and JJAS, as well as to understand the associated synoptic conditions. We pay special attention to the role of mid-latitude high-pressure structures, which are tracked here with the combined detection algorithm proposed by Sousa et al. (2021). This overcomes the limitations of the more restricted perspectives of blocking adopted by Ordóñez et al. (2017) and Otero et al. (2022), as it provides an integrated approach for the life cycle of high-pressure events, identifying subtropical ridges and different types of blocking patterns. To better understand the potential role of the atmospheric circulation in driving ozone episodes, we also introduce a novel circulation index that measures the similarity of mid-tropospheric meteorological anomalies on a given day and on episode days. A comprehensive set of chemical and meteorological fields from reanalysis datasets is also employed to shed light on the different factors that contribute to triggering large ozone episodes.

The paper is structured as follows. Section 2 describes the chemical and meteorological data utilized and the methodology applied to understand the processes associated with the occurrence of ozone episodes, including the main characteristics of the algorithm used for the detection of blocks and ridges. In Section 3 we identify the affected regions. Sections 4 and 5 examine the meteorological conditions and other factors governing the days with ozone episodes in those regions during AM and JJAS, respectively. Finally, Section 6 summarises and discusses the main conclusions of the study.

2. Data and methods

2.1. Chemical and meteorological data

The primary data source for this study is the catalogue of the 100 largest European ozone episodes during April–September 2003–2022 extracted by CM2024 from the CAMS global reanalysis (EAC4) dataset (Inness et al., 2019) at a horizontal resolution of 1.0° × 1.0°. As documented by CM2024, all episodes were ranked based on the integrated areal extents during their whole life cycles, and the 100 largest ones were selected for further analyses. According to the validation performed by the authors, CAMS shows good skill in capturing O_3 extremes (exceedances of the local 95th percentiles) when compared to an 1.0° × 1.0° hourly gridded observational ozone dataset that covers 2003–2015 (Schnell et al., 2014, 2015), particularly in areas with a high density of surface monitoring stations (see Section S2 in the supplementary material of CM2024). We have used the same dataset to evaluate the occurrence of local extremes within large episodes in CAMS during that period (see Section S1 of the Supplement). Overall, a high percentage of ozone extremes identified in CAMS are also present in the observational dataset (Fig. S1). Moreover, even though some extremes are not classified as observational extremes when using the strict 95th percentile threshold, they are consistently associated with high ozone percentiles in the observational record (Fig. S2).

Additionally, we have used 3-hourly atmospheric composition fields during April–September, including ozone, CO, nitrogen dioxide (NO_2), nitrogen monoxide (NO), formaldehyde (CH_2O), ethane (C_2H_6) and propane (C_3H_8) mixing ratios at the lowest model level from CAMS. Ozone data at 9 pressure levels (from 500 hPa to 1000 hPa) are also utilized. These datasets were downloaded at the same horizontal resolution as the catalogue of ozone episodes (i.e., 1.0° × 1.0°) for the period 2003–2022.

We have also used monthly anthropogenic emissions of some ozone precursors (NO_x, CO and NMVOCs) from the CAMS global emission inventory dataset (Granier et al., 2019). In addition, daily averages of wildfire radiative power and wildfire emission fluxes of NO_x, CO and NMVOCs from the CAMS Global Fire Assimilation System (GFAS) are used. GFAS utilises satellite observations of fire radiative power to provide near real-time information on the location, intensity, and estimated emissions from biomass burning and vegetation fires (Kaiser et al., 2012). We consider grid cells with wildfire radiative power values >0 W/m^2 as indicative of biomass burning occurrence, given that GFAS applies filtering procedures to exclude spurious signals, e.g. from non-biomass sources such as volcanoes, gas flares, and industrial activity as well as suspiciously large observations over extensive areas (Kaiser et al., 2012; CAMS, 2020). These datasets have been downloaded at their native horizontal resolution of 0.1° × 0.1°, which enables the identification of potential emission sources of interest.

To examine the typical meteorological conditions during the spring and summer months of 2003–2022 as well as under the presence of ozone episodes in that period, we use hourly ERA-5 reanalysis data (Hersbach et al., 2020). Again, for consistency with the catalogue of ozone episodes, these data have been downloaded at a horizontal resolution of 1.0° × 1.0°. The following variables are considered: 2-m temperature (T2M), sea level pressure (SLP), precipitation, horizontal wind at 850 hPa, vertical velocity at 500 hPa (ω500) and 500 hPa geopotential height (Z500). Daily maximum temperature has been computed as the maximum from all the hourly temperature values available for each day, and daily precipitation as the sum of 1-h accumulated precipitation values over 24-hour periods. Daily means of SLP, horizontal wind speed at 850 hPa, ω500 and Z500 are computed by averaging the instantaneous values at the standard meteorological hours 00, 06, 12 and 18 UTC for each day. Additionally, daily averages of 10-m and 500-hPa wind speed are combined with the accumulated precipitation to obtain the air stagnation index (ASI) following Horton et al. (2014). This index is employed to assess the occurrence of stagnant conditions during days with ozone episodes over specific regions. A grid cell is classified as stagnant on a given day if the average 10-m wind speed is <3.2 ms^{-1}, average 500-hPa wind speed is <13.0 ms^{-1} and total precipitation is <1 mm.

2.2. Methods

In the following sections we first identify the main regions in Europe affected by ozone episodes separately for AM and JJAS. A region is considered to be under the influence of an ozone episode on a given day if this covers at least one-third of the land grid cells. Subsequently, we analyse the associated meteorological conditions by using Z500, T2M and total precipitation anomalies, as well as wind speed composites. For each period (AM or JJAS), the anomalies are computed as the difference between a given meteorological field (or air pollutant concentrations) on ozone episode days in a specific region and the 2003–2022 climatology of that field for the corresponding period. The statistical significance of the anomalies is determined by using a bootstrap resampling method (10,000 iterations) at the 95 % confidence level. Anomalies are deemed significant when they fall outside the [2.5–97.5]th percentile range of the bootstrap distribution. We also apply the non-parametric two-sample Kolmogorov-Smirnov test to estimate whether the distributions of some meteorological fields and air pollutants under different conditions are significantly different at the 95 % confidence level.

Once the meteorological conditions associated with the occurrence of ozone episodes in a region have been identified, it is possible to examine how ozone concentrations respond on days with a similar meteorological pattern throughout the entire study period (AM or JJAS depending on the region). For this purpose, we construct a regional daily index I(Z500)^R by projecting the daily Z500 anomalies during the period of study (AM or JJAS 2003–2022) on the corresponding composite derived for O_3 episodes in the region. For a given day and region R, the index can be written as:

$$I(Z500)^R = \frac{< Z500_{daily}, Z500^R >}{< Z500^R, Z500^R >}$$

In this equation $Z500_{daily}$ is a two-dimensional matrix representing the Z500 anomaly field for a day, and $Z500^R$ represents the composite of the average Z500 anomaly field for days with ozone episode in the region (two-dimensional matrix with the same size as $Z500_{daily}$). The brackets denote the inner (dot) product of two fields. The index gives a measure of the resemblance between the synoptic patterns on that day and during ozone episode days. It is expected to have values close to 1 when the daily Z500 anomaly field ($Z500_{daily}$) resembles the typical anomaly pattern found for ozone episode days ($Z500^R$), near zero when both anomalies are not related, and around −1 when the anomalies are of similar magnitude but of opposite sign.

To understand the role of high-pressure systems as potential drivers of ozone episodes in the main affected regions, we use the combined detection algorithm proposed by Sousa et al. (2021). This algorithm considers the fact that subtropical ridges occasionally experience wave breaking, initiating the formation of blocking events, which often begin as omega-shape blocks connected to the subtropics (referred to as omega block). These systems may evolve into the north–south dipole pattern characteristic of Rex-pure blocks or display omega-Rex mixed features (referred to as Rex-hybrid blocks). The typical cycle of a ridge-block event, as identified by the algorithm, is illustrated in Fig. 1 by Sousa et al. (2021). The algorithm was applied to detect the day-to-day evolution of high-pressure structures during April–September 2003–2022 by using Z500 data from the ERA-5 reanalysis at 1.0° × 1.0° horizontal resolution. We generate a daily catalogue of blocks and ridges that lists their type (i.e., subtropical ridge, omega block, Rex-pure block, Rex-hybrid block) and characteristics (e.g., location, areal extent). Another relevant output of this algorithm is the poleward edge of the subtropical belt (LAT_{MIN}). LAT_{MIN} takes one value per day and is considered the minimum latitude for the formation of subtropical ridges and blocks. For

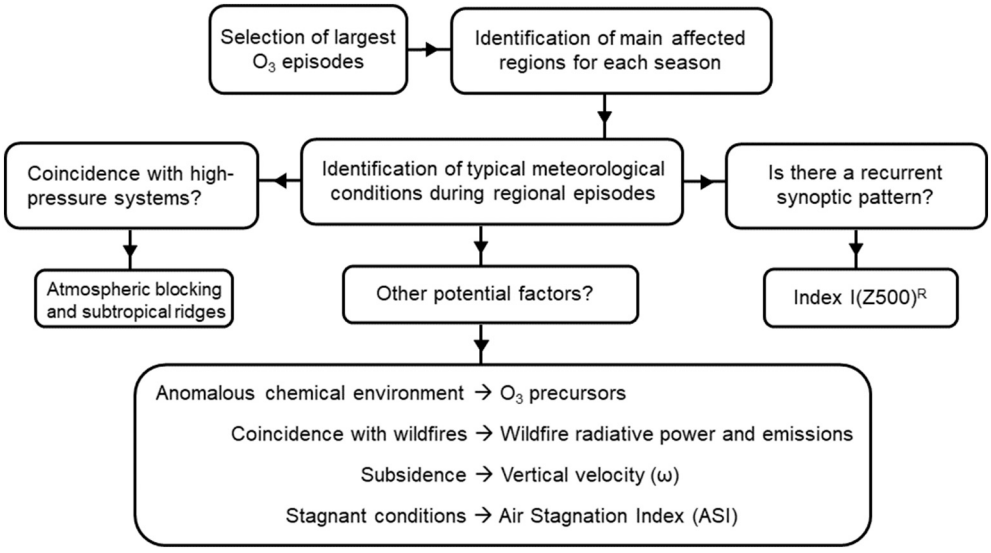

Fig. 1. Flowchart of the methodology used to understand the drivers of ozone episodes.

more details related to the algorithm see the original paper by Sousa et al. (2021).

A summary of the main methods used to understand the causes of regional ozone episodes is provided in Fig. 1. Briefly, for days with O_3 episodes in a region, maps of meteorological fields and anomalies are produced to identify the average synoptic patterns. Examining the coincidence with high-pressure systems and/or the application of the I(Z500)^R index provide further information on the importance of large-to-synoptic meteorological patterns. The influence of anomalous concentrations and/or emissions of precursors from different sources (including biomass burning), as well as the effect of other meteorological processes such as subsidence and air stagnation are also assessed. These factors are examined with a different degree of detail depending on the region.

3. Spatial distribution of the 100 largest ozone episodes

The spatial distribution of the 100 largest European ozone episodes during 2003–2022 is presented in Fig. 2. Episodes mainly affect regions north of around 48° N in AM (top panel) and south of 54° N in JJAS (bottom panel), as reported by CM2024. Note that the frequencies of episode occurrence are relatively low. This is because the detection of episodes is based on local exceedances of the 95th percentiles of daily O_3 maxima in April–September, with some additional conditions to merge these local extremes into episodes as mentioned in Section 1. Moreover, here we are analysing the 100 largest out of a total of 974 episodes found during the entire period. Ozone episodes in AM tend to cluster over the British Islands and a region covering large parts of eastern Europe and western Russia. In JJAS, episodes are concentrated in a large region spanning from western to eastern Europe, and extend to the south to cover Italy and the Balkans. The three regions are referred to hereafter as British Isles (BRIT), Eastern Europe (EEU) and Central Europe (CEU), respectively. A total of 38 days with ozone episodes affecting BRIT and 28 days in EEU were identified in AM, as well as 43 days in CEU during JJAS. The subsequent sections analyse the meteorological conditions during the days with ozone episodes in each period and region.

4. Ozone episodes in April–May

The synoptic conditions for the 38 days with ozone episodes found in BRIT during AM are shown in Fig. 3. They include negative anomalies of Z500 and T2M (panels a and b), above average precipitation (panel d) and stronger lower-troposphere winds over the region than in the climatology (panel c and upper panel of Fig. S3). These unusual synoptic patterns have not been reported previously for this region, where ozone episodes during the spring–summer months have been associated with high temperatures and stagnation of air masses as well as with southerly advection and import of pollution from continental Europe (Lee et al., 2006; Vieno et al., 2010; Pope et al., 2016; Carro-Calvo et al., 2017; Garrido-Perez et al., 2019).

In contrast, the 28 days with ozone episodes in EEU during AM are characterized by a well-defined pattern with positive anomalies of up to 8 °C for T2M, 6 hPa for SLP and 150 gpm for Z500 (Fig. 4 a, b). Precipitation deficits, recirculation of air masses and reduced wind speeds compared to the climatology in the centre of the anticyclonic circulation are also observed (Fig. 4 c, d and Fig. S3 top panel). Unlike the previous findings for BRIT, these conditions align with well-documented meteorological drivers of elevated ozone concentrations (e.g., Otero et al., 2016, 2022; Ordóñez et al., 2017). The contrasting results found for BRIT and EEU indicate that different processes trigger the occurrence of high ozone levels over these regions. In the remainder of this section, we will assess the role of high-pressure systems (blocking and ridges), advection, downward transport of air masses, and changes in the chemical regime as potential processes conducive to ozone episodes.

First, we have examined the local coincidences between ozone episodes and high-pressure structures. Fig. 5 illustrates the percentage of days with ozone episodes that coincide with blocks and ridges over each grid cell (see top panel for AM). There is good spatial correspondence over large parts of Europe which are excluded from the subsequent analyses because we aim to focus on the regions with the highest occurrence of ozone episodes, i.e., EEU and BRIT (top panel of Fig. 2). In particular, over the centre and south of EEU, ozone episodes often coincide with a block or ridge on the same day (30–80 % of the days depending on the grid cell). In contrast, this coincidence is below 30 % in the northern part of EEU and in BRIT. These results are not surprising in the case of BRIT given the negative Z500 anomalies associated with O_3 episode days in this region (Fig. 3a).

In addition to local coincidences, we have examined the co-occurrence of regional events for each box in Fig. 5. On a given day, we consider a regional concurrent (ozone and high-pressure) event to have occurred if both an ozone episode and a high-pressure system are affecting the region. For this, we have imposed two conditions: (1) as before, at least one third of the land grid cells in the region are affected by an ozone episode and (2) the centre of the block or ridge structure is located between 7.5° to the east of the eastern edge of the region and 7.5° to the west of the western edge. We use a broad area to detect

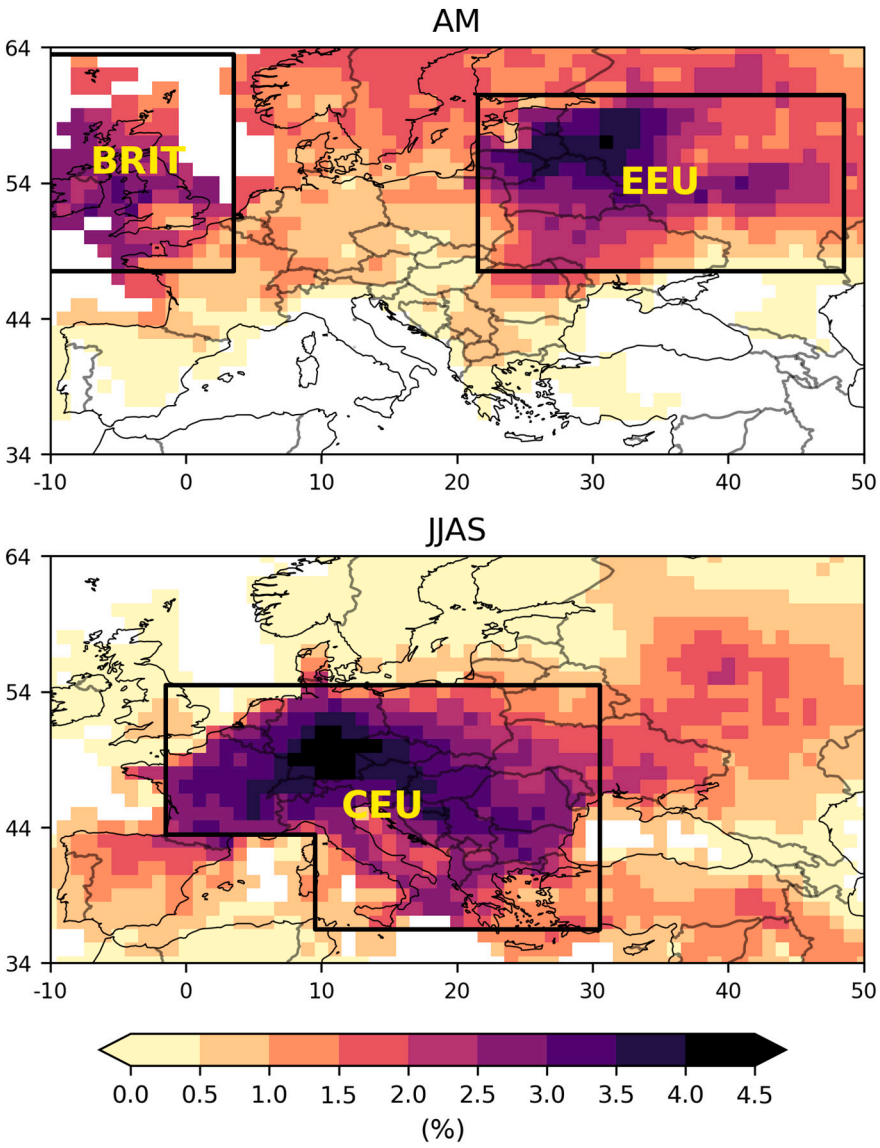

Fig. 2. Frequency of occurrence (% over the total number of days) of the 100 largest European ozone episodes during April–May (AM, top) and June–September (JJAS, bottom) of 2003–2022. The boxes indicate the location of the regions with the highest incidence of episodes: British Isles (BRIT) and eastern Europe (EEU) in AM and central Europe (CEU) in JJAS.

regional blocks and ridges, since these large-scale structures may affect a region even if their centres are located beyond its boundaries. Moreover, the 7.5° threshold used here is approximately half the minimum size of these structures. This analysis reveals two distinct regimes in the case of ozone episodes in BRIT: 10 episode days with a Rex block located north of the region and 28 episode days that are not clearly affected by any type of high-pressure system. As expected, in both cases the daily O_3 maxima averaged over the area exhibit considerably less spread than in the climatology, with median values increasing by approximately 7–10 ppb above the AM climatological median (Fig. 6).

The meteorological fields for the 10 episode days coinciding with a Rex block display positive Z500 and SLP anomalies well to the north of BRIT (Fig. S4, panels a and c). These days are also associated with negative Z500 and T2M anomalies over the southern half of BRIT and most of western Europe (consistent with Fig. 3), as well as with relatively strong easterly winds in the lower troposphere (panel e). In the southern half of the region, wind speeds at 850 hPa are around (11.3 ± 2.8) m/s (mean ± standard deviation), compared to (9.2 ± 2.9) m/s in the climatology. Overall, the concentrations of the main ozone precursors, i.e., NO_x and NMVOCs (calculated as the sum of formaldehyde, ethane and propane), are low on these days compared to the climatology, at least over the southern half of BRIT (Fig. 7, left and middle, and Fig. S5). Coinciding with the strong winds on days with Rex-block influence, NO_x anomalies reach −5 ppb and the median of the NMVOC concentrations is around 0.3 ppb below the climatological median. Note that most locations in BRIT are known to frequently exhibit a high-NO_x chemical regime, where reductions in NO_x emissions lead to increases in O_3 mixing ratios, and O_3 production increases with high NMVOCs emissions (Vieno et al., 2010; Liu et al., 2022). Consequently, these results suggest that the stronger-than-usual wind speed during these days ventilates the region, lowering NO_x and raising O_3 because of reduced titration by NO.

In contrast, the 28 days without Rex block influence in BRIT are typically characterized by a southwesterly-westerly flow extending over the North Sea and Scandinavia, wind speeds that fluctuate considerably from day to day (10.75 ± 4.9 m/s), and slight negative anomalies of Z500 and T2M over the region (Fig. S4, panels b, d, f). Most of these days are grouped into four distinct events, each lasting between 3 and 5 days. To understand the reasons behind them, we have examined maps of near-surface O_3 over the Euro-Atlantic sector; longitudinal-vertical cross

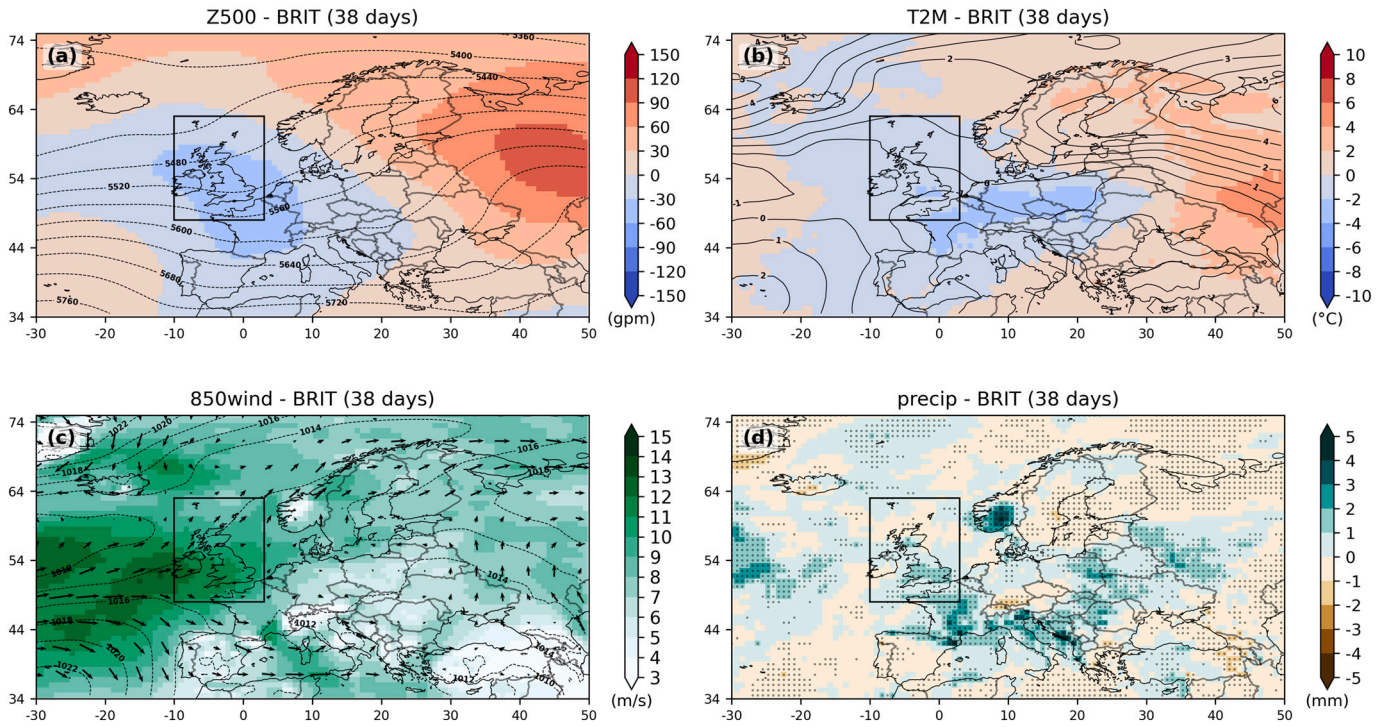

Fig. 3. Composites of daily meteorological fields, considering only days with ozone episodes in BRIT during AM 2003–2022: (a) anomalies (shaded) and mean values (black contour lines) of 500 hPa geopotential height (gpm), (b) temperature (shaded, °C) and sea level pressure (SLP) (black contour lines, hPa) anomalies, (c) module (green shaded, m/s) and vectors (arrows) of horizontal wind at 850 hPa as well as SLP (black contour lines, hPa) and (d) precipitation anomalies (mm). The black dots in a, b and d represent anomalies that are statistically significant at the 95 % level (determined through a bootstrap resampling method, see main text). The box indicates the region of study.

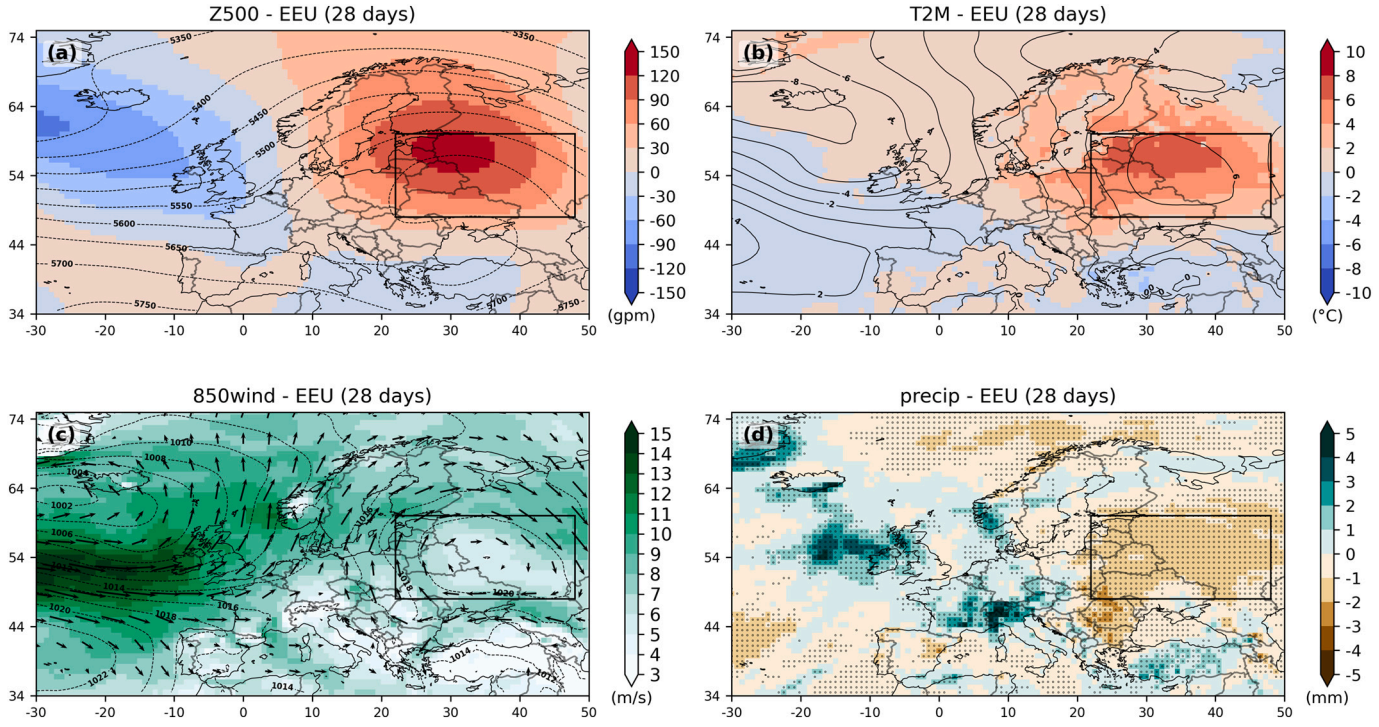

Fig. 4. As Fig. 3 but for ozone episodes in EEU during AM 2003–2022.

sections of O_3 in the mid- to lower-troposphere (500–1000 hPa) over BRIT; the evolution of the ω500 field, which indicates that there are both downward and upward movements in the region (positive and negative values, respectively), and some ancillary meteorological data. Overall, these analyses reveal that such episodes occur under varying dynamical conditions (not shown) and therefore cannot be attributed to a common cause. Further details are provided in Table S1. On the other hand, the levels of precursors remain low, ruling out a connection with enhanced

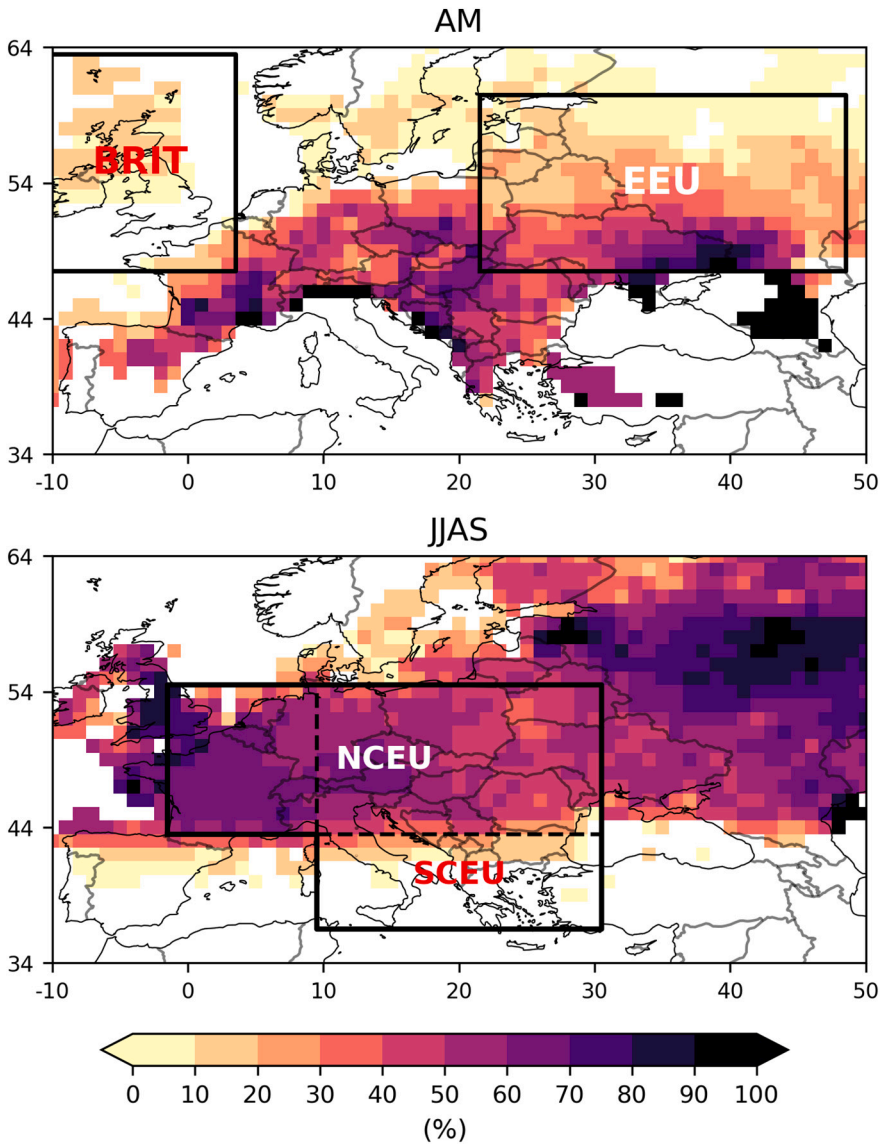

Fig. 5. Rate (%) of ozone episode days associated with blocks and ridges relative to the local mean frequency of ozone episodes in AM (top) and JJAS (bottom). The boxes with solid lines indicate the regions with the highest incidence of episodes as seen in Fig. 2: BRIT and EEU in AM and CEU in JJAS. In the bottom panel, the horizontal dashed line around 44°N divides CEU in two subregions: NCEU to the north and SCEU to the south. In addition, the vertical dashed line around 10°E separates the western and eastern portions of NCEU.

photochemistry as in the case of Rex block. In particular, NO_x anomalies are slightly negative over most of England, reaching −5 ppb along the British Channel and the southern part of the North Sea (Fig. 7 right panel), and daily NMVOC levels remain below the climatological values over the whole region (Fig. S5).

These findings suggest that, in the absence of a favourable Z500 pattern or high temperatures, advection is the process that favours the occurrence of ozone episodes in BRIT. Under Rex-blocks influence, strong easterly winds ventilate the region. On the other hand, no common pattern is observed for episodes without Rex-block influence. As indicated above, these results for the spring months contrast with the known association of high ozone levels in the region with anticyclonic conditions and with the transport of polluted air masses from continental Europe during spring-summer (Jenkin et al., 2002; Lee et al., 2006; Pope et al., 2016; Carro-Calvo et al., 2017; Garrido-Perez et al., 2019; Romero-Alvarez et al., 2025).

Unlike BRIT, the Z500 anomaly field exhibits a clear anticyclonic pattern on the 28 days with episodes in EEU (Fig. 4a). The median of daily O_3 maxima averaged over the region during those days is 52 ppb, compared to 45 ppb in the AM climatology (Fig. 6). Although the blocking and ridges algorithm detected high-pressure patterns in the proximity of the region only on five of the episode days (see also Fig. 5), strong positive Z500 anomalies over the region are still observed for the remaining 23 days (not shown). Following these results, two questions remain: (i) whether the pattern from Fig. 4a is recurrent in AM, and (ii) to what extent it is essential for the occurrence of ozone episodes in this region. To understand this, we employ the $I(Z500)^R$ index which is calculated for each day in AM 2003–2022 over the domain [34°–74° N, 0°–50° E]. A day is considered to resemble that pattern if the index takes a value equal or close to 1.

To address the first question, we have selected the central tercile from the daily distribution of $I(Z500)^R$ values on ozone episode days in the region as an indicator of a Z500 reference pattern like the one from Fig. 4a. This corresponds to index values within [0.6, 1.3]. Then, we have looked for all days in AM 2003–2022 with $I(Z500)^R$ values within that range and identified 187 out of 1220 days. This corresponds to 15 % of the days, which is considerably higher than the number of days with ozone episodes (28, i.e. 2 % of all days). These results indicate that EEU

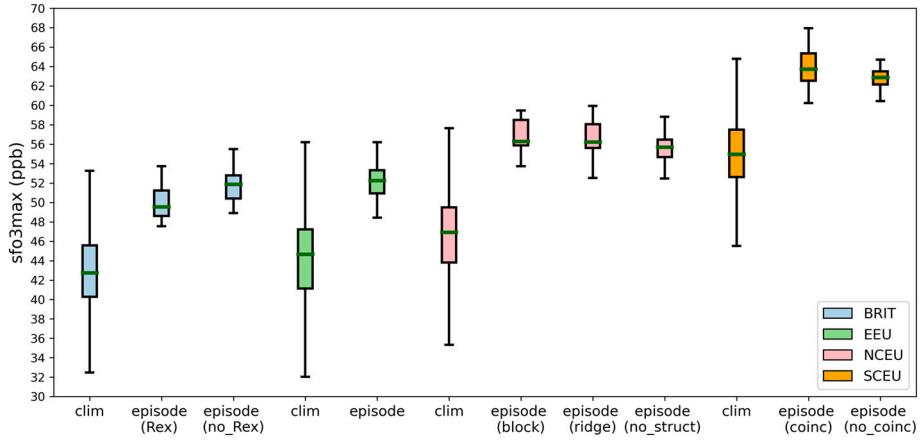

Fig. 6. Averages of daily ozone maxima over the regions of study for the corresponding climatology (AM or JJAS, labelled as clim) during 2003–2022 and for days with ozone episode in those regions and periods (labelled as episode): days with episode in BRIT coinciding with a Rex block (episode (Rex)) and without a Rex block (episode (no_Rex)); days with episode in EEU (episode); days with episode in NCEU coinciding with a block (episode (block)) or a subtropical ridge (episode (ridge)), and without anticyclonic structures (episode (no_struct)); days with episode in SCEU that also affect NCEU (episode (coinc)) and days with episode only in SCEU (episode (no_coinc)). The boxes extend from the lower (Q1) to upper (Q3) quartile values of the data, with a horizontal green line indicating the position of the median. The whiskers extend from the box to show the range of the data, from a minimum value up to (Q1–1.5 IQR) to a maximum value up to (Q3 + 1.5 IQR) (IQR = Interquartile range).

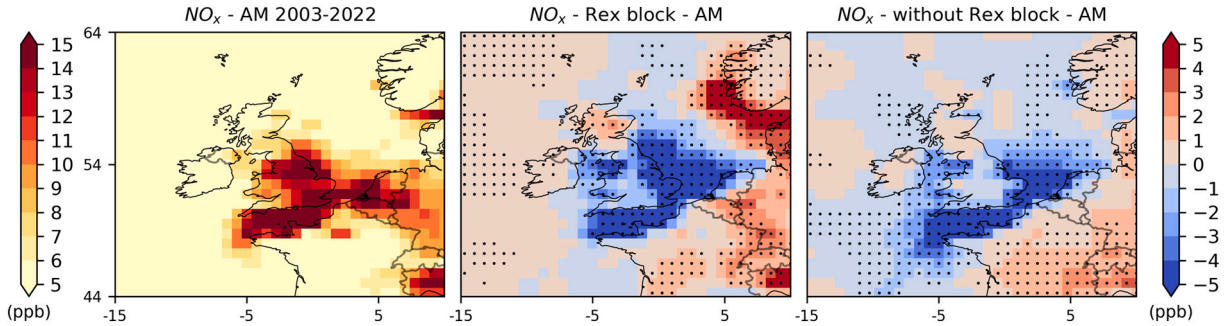

Fig. 7. Average NO_x concentrations during AM 2003–2022 (left) and NO_x concentration anomalies for days with ozone episode coinciding with Rex block (easterly winds, middle) and without Rex block (right) in BRIT for the same period. The black dots in the middle and right panels represent anomalies that are statistically significant at the 95 % level (determined through a bootstrap resampling method).

is with some regularity influenced by a similar Z500 pattern during AM and that this pattern alone is not a sufficient condition for the occurrence of ozone episodes. Additionally, we have examined the concentrations of O_3 and the main precursors (CO, NO_x and NMVOCs) under three different conditions: (1) days with a Z500 pattern very close to the reference from Fig. 4a, (2) the 28 days with ozone episode in EEU, and (3) the remaining days in AM 2003–2022. For the first condition, we selected the 30 days with the index values closest to 1 to have a sample size comparable to the number of ozone episode days. Fig. S6 illustrates the concentrations of ozone and the main precursors for the three conditions. As shown in panel a, this Z500 pattern contributes to raising O_3 in AM, shifting the distribution toward higher O_3 levels compared to that of the rest of the days. However, on days with a favourable Z500 pattern, ozone concentrations are considerably lower than on ozone episode days. This supports our previous finding that the Z500 pattern is a favourable but not sufficient condition for the occurrence of an ozone episode in the region.

The concentrations of precursors are notably higher on ozone episode days than under the other conditions (Fig. S6, panels b, c, and d). Most of the days with episode in the region come into three major ozone events, consisting of 22 non-consecutive days concentrated in late April and early May of 2006, 2009 and 2013. During ozone episodes, wildfires are considerably more frequent than on the rest of the days in AM (Fig. S7), suggesting a meaningful contribution from biomass burning emissions. Fig. 8 (left column) shows the average anthropogenic emissions of NO_x, CO, and NMVOCs during AM 2003–2022, alongside the wildfire emission fluxes for the same species on days without ozone episodes (middle column) and on episode days (right column). Notably, wildfire fluxes exceed the mean anthropogenic emissions over large areas during episode days, particularly for CO. This is in line with previous studies identifying eastern Europe and the European part of Russia as regions prone to wildfire activity, particularly in spring (April–May). It is known that these events are driven by anthropogenic practices, such as dry grass burning on agricultural lands, and are also favoured by the co-occurrence of persistent blocking and high temperatures. They are recognised as significant sources of ozone precursors (mainly CO and, to a lesser extent, CH_4 and NO_x) and $PM_{2.5}$ (Bondur et al., 2020, and references therein). We can conclude that the simultaneous occurrence of both high-pressure conditions and high precursor emissions, often associated with wildfires, are required to trigger large ozone episodes in EEU during AM.

5. Ozone episodes in June–September

The average synoptic patterns for the 43 days with ozone episodes identified in CEU during JJAS reveal predominantly high-pressure conditions with moderate positive anomalies of Z500 (Fig. 9a). The episodes are linked to a ridge pattern, accompanied by positive T2M anomalies of up to ~8 °C and precipitation deficits over the region (panels b and d). During these days, the centre of the Azores High

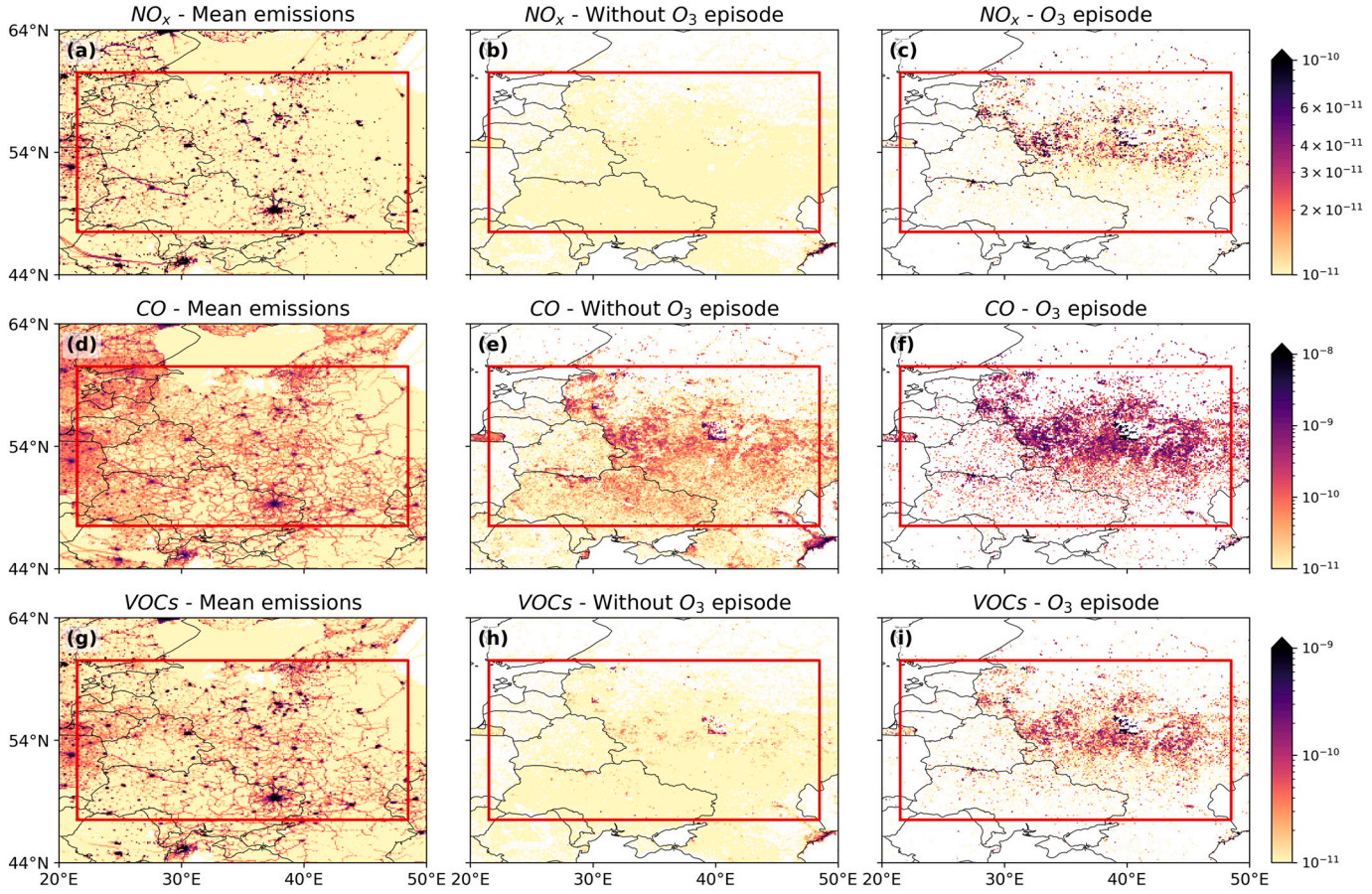

Fig. 8. Composites of monthly average anthropogenic emissions of main ozone precursors (kg m^{-2} s^{-1}, left column) and daily wildfire fluxes (kg m^{-2} s^{-1}) averaged over days without episode (middle column) and with episode (right column) in EEU during AM 2003–2022: (a–c) NO_x, (d–f) CO and (g–i) NMVOCs. The red boxes in all panels indicate the region of interest, i.e. EEU.

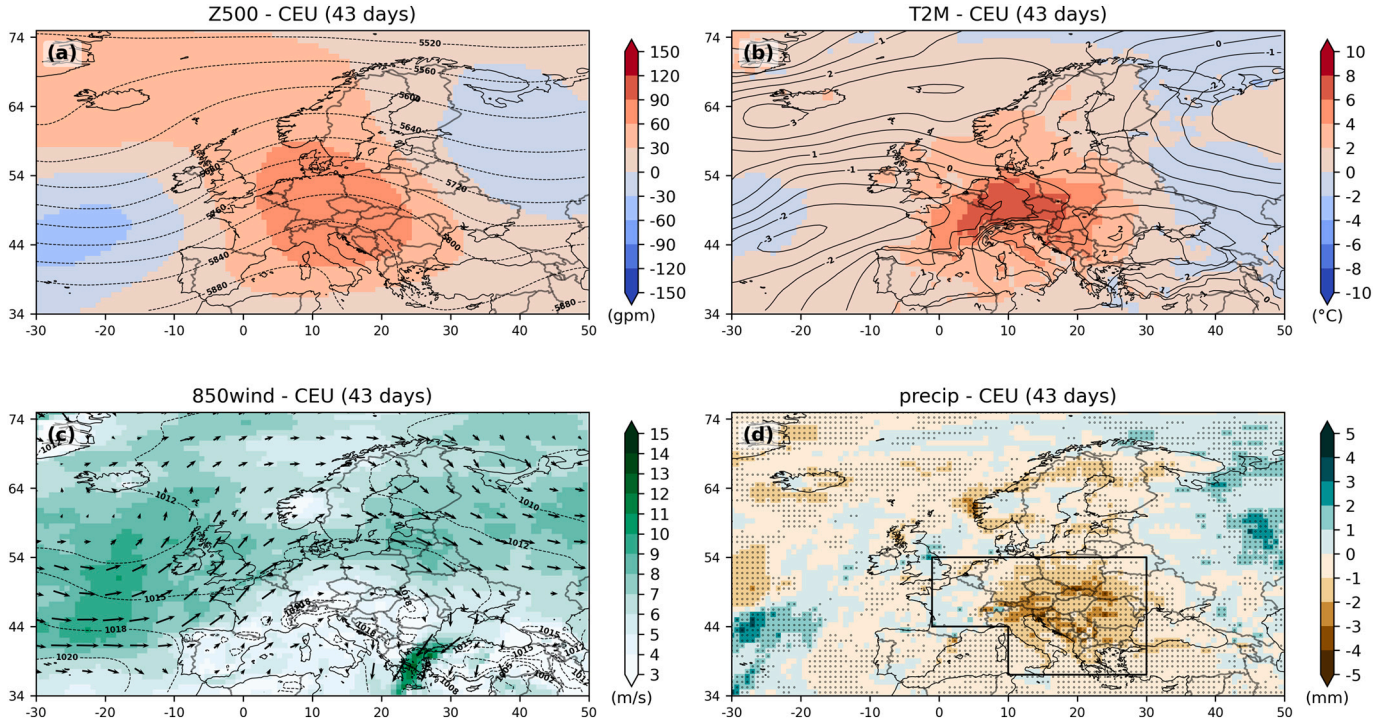

Fig. 9. As Fig. 3 but for ozone episodes in CEU during JJAS 2003–2022.

retreats toward the southwest in the Atlantic Ocean and the wind direction deviates from the typical zonal flow, with a southwesterly inflow upwind the region and northwesterly outflow downwind (Fig. 9c and bottom panel of Fig. S3).

As in AM, we have examined the local coincidences of ozone episodes with high-pressure systems in JJAS (Fig. 5 bottom panel). These coincidences are high north of 44° N, where 40–90 % of days with episodes are associated with the presence of blocks or ridges, except for a region around Scandinavia and the Baltic. One of the regions with the highest co-occurrence is western Russia. However, this is a region with lower incidence of summer ozone episodes than CEU (Fig. 2 bottom panel). Indeed, the percentage of days with episode there decreases considerably if we exclude the widely studied mega-heatwave of summer 2010 (see Fig. S8), which lasted 30 days and was linked to a quasi-stationary anticyclonic circulation over western Russia (Barriopedro et al., 2011; CM2024). As the focus of this study is not on individual events but on the regions with the highest occurrence, in the remainder of the section we only address episodes that affect CEU.

South of 44°N, there is no good correspondence between ozone episodes and high-pressure systems. This region is often located inside the subtropical belt during JJAS, as verified with the LAT_{MIN} diagnostic provided by the blocking and ridge algorithm. We found that LAT_{MIN} is located north of 43°N on more than 50 % of the days in JJAS. This implies that southern CEU is not directly affected by blocks or ridges during those days, as LAT_{MIN} marks the minimum latitude for the formation of blocks and subtropical ridges. Because of this, we have conducted separate analysis of ozone episodes in two subregions of CEU: the one north of 44°N (NCEU), at latitudes where high-pressure structures form, and the one south of 44°N (SCEU), mostly inside the subtropical belt. Note that when performing the analysis separately for these two subregions, the number of days with regional ozone events in any of them may be higher than the 43 events found for CEU. This is because we are now evaluating the occurrence of events in smaller regions, making it more likely to meet the previously established condition that at least one-third of the ozone episode must affect the region.

As expected, 60 % of the regional ozone episode days in NCEU coincide with a high-pressure structure. Specifically, out of a total of 60 days with episode, 13 are associated with blocks and 23 with ridges. Even on the 24 days where no structures are detected by the algorithm, positive Z500 anomalies are observed (Fig. S9a–c). There are some differences among the three situations (block, ridge, and no structure). The highest Z500 and T2M anomalies are found for days influenced by blocks (Fig. S9a–f), which also coincide with the weakest wind speeds and strongest precipitation deficits across the entire region (Fig. S9g–l). By far, the weakest meteorological anomalies occur on days without high-pressure structures. Despite this, the daily maximum O_3 concentrations averaged over the whole region remain similar across all synoptic configurations, with an increase of ~10 ppb in the median value compared to the climatology (Fig. 6). There are however some regional differences, as the highest local ozone exceedances above the 95th percentile reach 19 ppb on days influenced by blocks, compared to 13 ppb on days with ridges and 7 ppb on days without structure (Fig. 10). These results are consistent with the strong (weak) anomalies seen in the meteorological fields for ozone episodes with blocks (no high-pressure structure).

The highest O_3 levels in April–September 2003–2022 (both in the climatology and during episodes) are found in SCEU (Fig. 6). Because of the meridional extension of ridges and blocks, the high-pressure structures observed during O_3 episodes in NCEU may also be behind some of the episodes impacting SCEU, even if this region is inside the subtropical belt. Accordingly, we have conducted separate analyses for the episodes that simultaneously affect SCEU and the eastern part of NCEU (east of 10°E in Fig. 5 bottom panel) and those occurring solely in SCEU. The ozone distributions for days with episode differ from the climatology in both cases, with median values that exceed the climatological median by 8 ppb. Some of the 25 days with episodes occurring simultaneously in

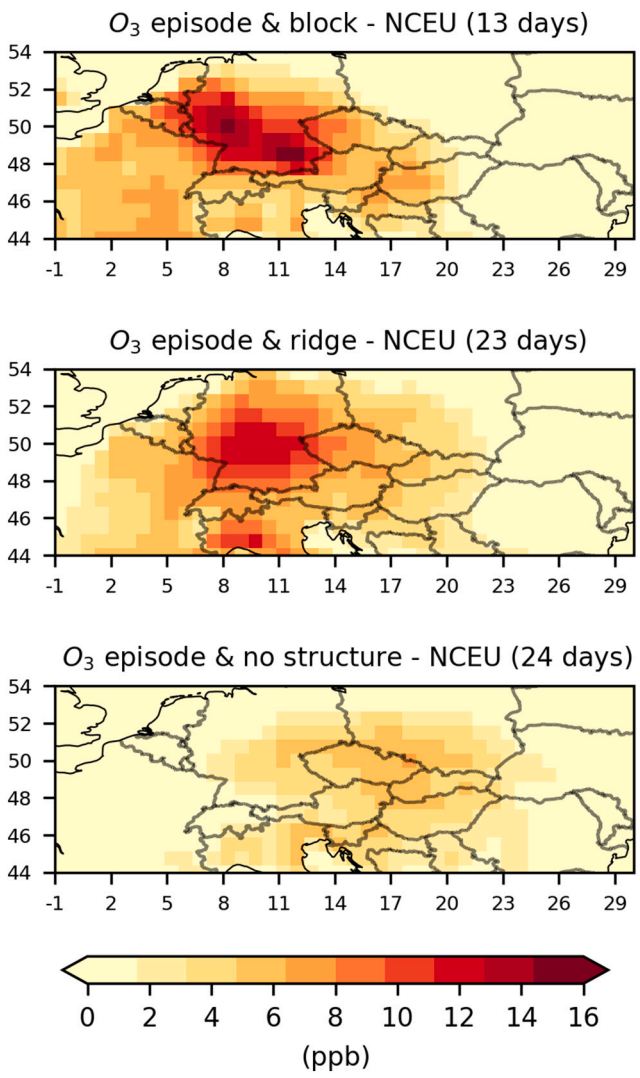

Fig. 10. Exceedances of daily ozone maxima above the local 95th percentiles for ozone episode days in NCEU during JJAS 2003–2022 grouped in three categories: (top) coinciding with blocks, (middle) coinciding with ridges and (bottom) rest of episode days.

both subregions reach the highest O_3 concentrations reported over SCEU. In this case, we have found positive Z500 and T2M anomalies, with the highest values located north of SCEU (Fig. S10 a, c), which are also symptomatic of high ozone levels in NCEU. In contrast, on the 29 days with episodes restricted to SCEU, there are weak positive anomalies of Z500 and T2M over the region and negative Z500 anomalies in the north (Fig. S10 b, d). Therefore, the near-surface wind exhibits a more zonal pattern to the north of SCEU compared to the other case (Fig. S10 e, f). Although the meteorological conditions in both cases favour ozone episodes, the Z500 and T2M anomalies associated with episodes occurring exclusively in SCEU are not particularly strong. Consequently, we have evaluated the potential influence of other factors, such as subsiding motions, air mass stagnation or anomalously high emissions, which, together with the moderate Z500 and T2M anomalies, may contribute to increased O_3 levels in SCEU. There is some evidence that these processes may be relevant over the region. The findings of Ziv et al. (2004), Horton et al. (2014) and Garrido-Perez et al. (2018) indicate that subsiding motions and air mass stagnation are common meteorological features over the eastern Mediterranean in summer. Ziv et al. (2004) noted that this region experiences tropospheric subsidence during the summer months, which plays a key role in local ozone formation and in the downward transport of ozone form the upper troposphere and

lower stratosphere (Doche et al., 2014; Zanis et al., 2014). Furthermore, SCEU is often characterized by stagnant conditions (Horton et al., 2014; Garrido-Perez et al., 2018) and by wildfire events (Li et al., 2024; Ochoa et al., 2024) during the summer months, which may be related to high ozone levels.

The analysis of ω500 confirms that SCEU is located on the northern edge of a broader region characterized by large-scale subsidence over the eastern Mediterranean during JJAS (Fig. S11). Indeed, the distribution of daily ω500 averaged over SCEU shows positive values on 87 % of the days and negative on the remaining 13 % (Fig. 11a). This distribution becomes consistently positive during ozone episode days, regardless of if they are restricted to SCEU or common with the eastern part of NCEU, indicating enhanced subsidence in both cases. In contrast, no significant deviations from the climatology are observed for stagnant conditions, wildfire activity, or NO_x levels during episode days restricted to SCEU. Specifically, the percentage of stagnant land grid cells during ozone episodes exclusive to this region does not significantly differ from the climatological values, although the frequency of stagnation increases for episodes common to SCEU and eastern NCEU (Fig. 11b). Of the three major ozone episodes found (each lasting between 3 and 7 days), only one of them shows an association with wildfire activity (not shown). Moreover, NO_x concentrations during episode days are comparable to the climatological values, while NMVOC levels tend to be higher but with more spread than the climatology (Fig. 11c, d), suggesting a possible contribution to ozone formation during some days. Overall, these results indicate that, in addition to the typical meteorological conditions, namely weak winds and modest positive anomalies of T2M and Z500, subsidence is a key mechanism driving the occurrence of ozone episodes in SCEU during JJAS.

6. Summary and discussion

This study has examined the spatial distribution and meteorological conditions associated with the 100 largest surface ozone episodes over Europe in the CAMS reanalysis during April–September 2003–2022. For that purpose, we have employed the catalogue of ozone episodes by CM2024, the detection algorithm for blocking and subtropical ridges by Sousa et al. (2021) and chemical and meteorological data from the CAMS and ERA-5 reanalyses, respectively. We found that ozone episodes tend to cluster over the British Islands (BRIT) and large parts of Eastern Europe (EEU) in April–May (AM) as well as over a large region including Central Europe (CEU) during June–September (JJAS).

The meteorological conditions and the dynamical processes contributing to high ozone levels vary across regions. In EEU, ozone episodes are concentrated in late April and early May. They are typically associated with well-defined anticyclonic conditions, characterized by positive anomalies of Z500 and T2M, recirculation of air masses and precipitation deficits. However, the presence of such a synoptic pattern alone does not seem to be sufficient to trigger ozone episodes. Our findings indicate that elevated concentrations of ozone precursors (CO, NO_x, and NMVOCs), largely linked to biomass burning, also play a crucial role in the development of the episodes. These results contribute to a better understanding of the mechanisms triggering high ozone concentrations in this region, where there is a lack of comprehensive studies for spring, and the focus has often been placed on the role of wildfires during the heatwave of summer 2010 (Konovalov et al., 2011; Péré et al., 2015).

In contrast, to the best of our knowledge, ozone episodes in BRIT during AM occur under meteorological conditions not previously

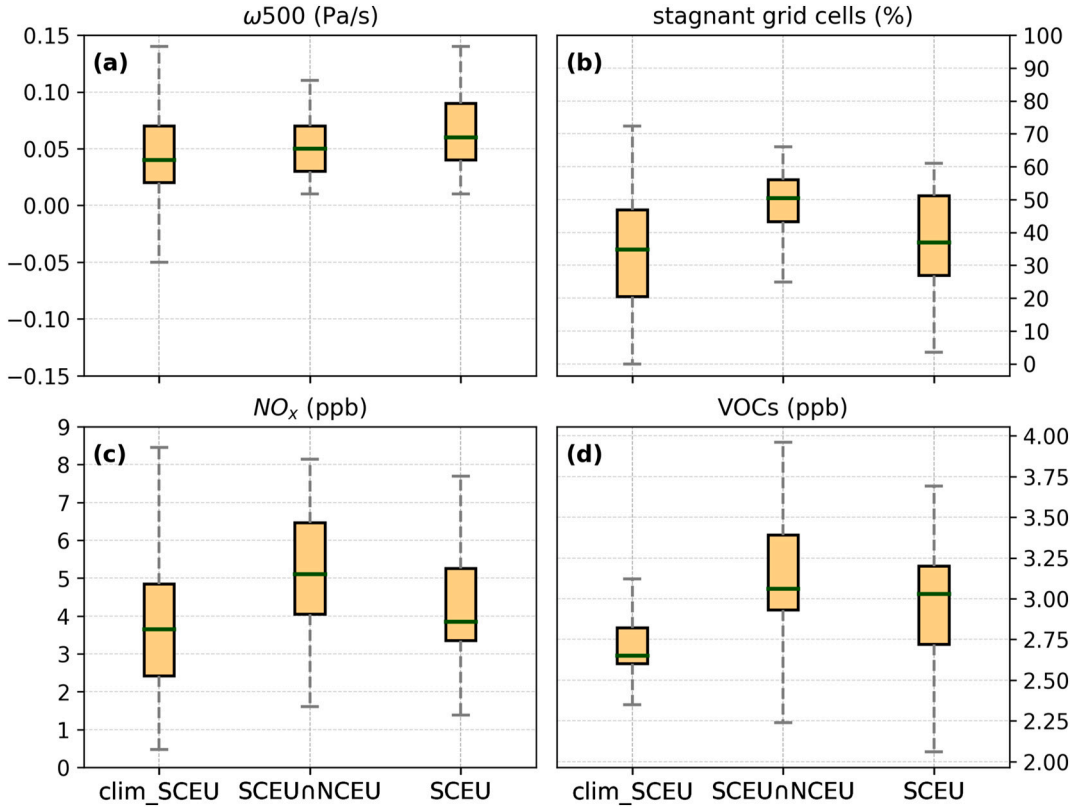

Fig. 11. Distributions of (a) vertical velocity at 500 hPa (Pa/s), (b) percentage of stagnant land grid cells (percentage), and (c) NO_x (ppb) and (d) NMVOC (calculated as the sum of CH_2O, C_2H_6 and C_3H_8, ppb) mean concentrations in SCEU. They are shown for all days in JJAS 2003–2022 (clim_SCEU), as well as days with ozone episodes coinciding in the eastern part of NCEU and SCEU (SCEU∩NCEU) and days with ozone episodes only in SCEU (SCEU) during the same period. Positive values on panel (a) represent subsidence, which is a recurrent feature on days with ozone episode. According to the two-sample Kolmogorov-Smirnov test, the other distributions (stagnant grid cells, NO_x and NMVOCs) for the days with ozone episodes common to the eastern part of NCEU and SCEU differ significantly from the climatology (p-value < 0.01). The same applies to the NMVOCs distribution for days with ozone episodes only in SCEU.

reported in the literature, featuring negative Z500 and T2M anomalies, stronger than usual winds, and positive precipitation anomalies. Our results indicate two distinct regimes: approximately one-quarter of the ozone episodes in BRIT are associated with a Rex block north of the region, while the remaining three-quarters present different synoptic conditions. In the first case, strong advection from the east plays a key role in the formation of high ozone levels by ventilating the region, reducing precursor concentrations and limiting ozone titration by NO. The other episodes do not exhibit a common synoptic pattern. Instead, they develop under varying meteorological conditions that result in distinct flow regimes. These situations differ from the spring–summer ozone enhancements over BRIT which have been attributed to high-pressure systems and to the transport of polluted air masses from continental Europe (Jenkin et al., 2002; Lee et al., 2006; Pope et al., 2016; Romero-Alvarez et al., 2025). The comparison of some spring and summer ozone episodes is not straightforward, given the seasonal differences in NO_x levels (on average ~1.4 ppb higher in spring than in summer over the region according to the CAMS reanalysis) and the non-linear response of O_3 to emissions. Dedicated source attribution (e.g., Lupaşcu et al., 2022, and references therein) and Lagrangian (e.g., Soleimanian et al., 2023) approaches tagging source regions could be very valuable to understand how dynamical processes interact with emissions and background concentrations to trigger ozone episodes in BRIT and other regions of northern Europe during spring.

Regarding ozone episodes in CEU during JJAS, we identified significant differences between the northern and southern parts of the region. In the northern subregion (NCEU), blocking and ridges are present on 60 % of the episode days, creating favourable conditions for ozone formation, such as positive Z500 and T2M anomalies, weak winds, and precipitation deficits. The highest ozone concentrations are observed with the presence of blocking and, to a lesser extent, ridges. These findings provide further evidence for a strong link between the large-scale circulation and large ozone episodes across a broad region around central Europe, in line with the results from previous studies (e.g., Ordóñez et al., 2017; Carro-Calvo et al., 2017; Otero et al., 2016, 2022). In contrast, the southern subregion (SCEU) is frequently located within the subtropical belt but is also under the influence of blocking and ridges, albeit less significantly. Ozone episodes in this subregion occur in the presence of weak winds and slightly positive Z500 and T2M anomalies. Even with moderate meteorological anomalies, the highest O_3 levels are found in SCEU, arguably due to mid-tropospheric subsidence, which is systematically present over this area during all episode days. Our results confirm the key role of this process in promoting high surface ozone concentrations over the Eastern Mediterranean under favourable meteorological conditions, as indicated by previous studies (Doche et al., 2014; Zanis et al., 2014). On the other hand, although a few studies have highlighted the importance of air stagnation in this region (e.g., Horton et al., 2014; Garrido-Perez et al., 2018, 2019), our results do not confirm it as a conditioning factor for the occurrence of large-scale ozone episodes restricted to SCEU. However, we find that the frequency of stagnation increases significantly above the climatological values when episodes simultaneously affect this region and NCEU.

We note that this analysis relies on atmospheric composition data from the CAMS global reanalysis (EAC4). While this dataset provides consistent long-term records, it is subject to inherent uncertainties both in the Integrated Forecasting System (IFS) and in data assimilation techniques. The assimilation of observational data for O_3, NO_2, CO and aerosols improves the skill of the IFS model in reproducing ozone concentrations (Inness et al., 2019; Sekiya et al., 2025). Indeed, the CAMS reanalysis has been shown to exhibit lower biases than other atmospheric composition reanalyses for near-surface ozone, in particular over Europe (Jones et al., 2025). Moreover, we have found a reasonably good correspondence between local ozone extremes identified in CAMS and those observed at the surface. However, constraining chemical fields in the model through data assimilation techniques may limit our ability to capture and interpret some of the processes responsible for ozone episodes as compared to a free run. Despite this, as shown above, we have overall reported consistent patterns for episode formation in the different regions.

Until now, only few comprehensive studies had examined the characteristics of large-scale ozone episodes in Europe. They employed a traditional Eulerian framework (e.g., Carro-Calvo et al., 2017) or a semi-Lagrangian approach (Schnell et al., 2014, 2015; CM2024), which remains less common in the literature. This study builds on the latter analyses, which mainly focused on the typical climatological features of ozone episodes. CM2024 also showed that the 10 largest episodes since 2003 broadly corresponded to well-documented heatwaves in the literature, in association with positive anomalies in Z500, daily maximum temperatures, and solar radiation; however, their investigation was restricted to individual episodes. The regional focus of this analysis goes beyond those studies by underscoring the importance of both synoptic-scale meteorological conditions and precursor emissions in driving large ozone episodes across different European regions. While high-pressure structures and stagnant conditions favour ozone accumulation, advection, subsidence and anomalous precursor emissions also play critical roles depending on the region. The methodology (see flowchart in Fig. 1) and findings presented here provide a comprehensive framework for understanding the interplay between meteorology and ozone episodes, which is essential for air quality management and future climate projections. We are aware that this is a regional study for Europe, so other processes that are not represented in Fig. 1 may be considered to understand the drivers of large ozone episodes in other mid-latitude regions like North America and Eastern Asia. On the other hand, according to the current state of knowledge, the future evolution of near-surface O_3 in Europe will be strongly determined by the evolution of precursor emissions, including methane, and to a lesser extent by climate change (Fortems-Cheiney et al., 2017; Turnock et al., 2022; CM2024). However, there is strong interannual variability in the projections of future ozone episodes (CM2024), which are expected to be linked to fluctuations in meteorological conditions. Future work should assess whether the role of the key drivers of regional ozone episodes identified in this study remains in future scenarios with different degrees of climate forcing and air pollution control.

CRediT authorship contribution statement

Tahimy Fuentes-Alvarez: Writing – original draft, Visualization, Formal analysis. **Carlos Ordóñez:** Writing – review & editing, Supervision, Project administration, Methodology, Funding acquisition. **Ricardo García-Herrera:** Writing – review & editing, Project administration, Methodology, Funding acquisition. **David Barriopedro:** Writing – review & editing, Methodology. **Rodrigo Crespo-Miguel:** Writing – review & editing, Software, Visualization. **Miguel M. Lima:** Writing – review & editing, Software.

Declaration of competing interest

The authors declare that they have no known competing financial interests or personal relationships that could have appeared to influence the work reported in this paper.

Acknowledgements

This work is supported by MALONE (PID2021-122252OB-I00), project funded by MICIU/AEI/10.13039/501100011033 and ERDF, EU. TFA is supported by a predoctoral research fellowship funded by the Ministry of Science and Innovation (PRE2022-101985). MML is supported through the PhD MIT Portugal MPP2030-FCT programme by project reference and DOI identifier doi:10.54499/PRT/BD/154680/2023. The authors acknowledge the European Centre for Medium-Range Weather Forecasts for the provision of CAMS and ERA5 reanalysis data. The authors thank two anonymous referees for

providing insightful and constructive comments on the original draft.

Appendix A. Supplementary data

Supplementary data to this article can be found online at https://doi.org/10.1016/j.scitotenv.2025.180578.

Data availability

CAMS and ERA5 reanalysis data used in this work are publicly available.

References

Atkinson, R., 2000. Atmospheric chemistry of VOCs and NO_x. Atmos. Environ. 34, 2063–2101. https://doi.org/10.1016/S1352-2310(99)00460-4.

Barriopedro, D., Fischer, E.M., Luterbacher, J., Trigo, R.M., García-Herrera, R., 2011. The hot summer of 2010: redrawing the temperature record map of Europe. Science 332. https://doi.org/10.1126/science.1201045.

Bloomfield, P., Royle, J.A., Steinbergt, L.J., Yang, Q., 1996. Accounting for meteorological effects in measuring urban ozone levels and trends. Atmos. Environ. 30 (17), 3067–3077. https://doi.org/10.1016/1352-2310(95)00347-9.

Boleti, E., Hueglin, C., Grange, S.K., Prévôt, A.S.H., Takahama, S., 2020. Temporal and spatial analysis of ozone concentrations in Europe based on timescale decomposition and a multi-clustering approach. Atmos. Chem. Phys. 20, 9051–9066. https://doi.org/10.5194/acp-20-9051-2020.

Bondur, V.G., Voronova, O.S., Cherepanova, E.V., Tsidilina, M.N., Zima, A.L., 2020. Spatiotemporal analysis of multi-year wildfires and emissions of trace gases and aerosols in Russia based on satellite data. Izv., Atmos. Ocean. Phys. 56 (12), 1457–1469. https://doi.org/10.1134/S0001433820120348.

Booker, F., Muntifering, R., McGrath, M., Burkey, K., Decoteau, D., Fiscus, E., Manning, W., Krupa, S., Chappelka, A., Grantz, D., 2009. The ozone component of global change: potential effects on agricultural and horticultural plant yield, product quality and interactions with invasive species. J. Integr. Plant Biol. 51 (4), 337–351. https://doi.org/10.1111/j.1744-7909.2008.00805.x.

Carro-Calvo, L., Ordóñez, C., García-Herrera, R., Schnell, J.L., 2017. Spatial clustering and meteorological drivers of summer ozone in Europe. Atmos. Environ. 167, 496–510. https://doi.org/10.1016/j.atmosenv.2017.08.050.

Copernicus Atmosphere Monitoring Service, 2020. Global Fire Assimilation System (GFAS) v1.2: Data documentation. European Centre for Medium-Range Weather Forecasts. Available from. https://atmosphere.copernicus.eu (last accessed 02/05/2025).

Crespo-Miguel, R., Ordóñez, C., García-Herrera, R., Schnell, J.L., Turnock, S.T., 2024. Large-scale ozone episodes in Europe: decreasing sizes in the last decades but diverging changes in the future. Sci. Total Environ. 949. https://doi.org/10.1016/j.scitotenv.2024.175071.

Demuzere, M., Trigo, R.M., Vila-Guerau De Arellano, J., van Lipzig, N.P.M., 2009. The impact of weather and atmospheric circulation on O_3 and PM_{10} levels at a rural mid-latitude site. Atmos. Chem. Phys. 9, 2695–2714. https://doi.org/10.5194/acp-9-2695-2009.

Doche, C., Dufour, G., Foret, G., Eremenko, M., Cuesta, J., Beekmann, M., Kalabokas, P., 2014. Summertime tropospheric-ozone variability over the Mediterranean basin observed with IASI. Atmos. Chem. Phys. 14, 10589–10600. https://doi.org/10.5194/acp-14-10589-2014.

Fortems-Cheiney, A., Foret, G., Siour, G., Vautard, R., Szopa, S., Dufour, G., Colette, A., Lacressonniere, G., Beekmann, M., 2017. A 3 °C global RCP8.5 emission trajectory cancels benefits of European emission reductions on air quality. Nat. Commun. 8, 89. https://doi.org/10.1038/s41467-017-00075-9.

Garrido-Perez, J.M., Ordóñez, C., García-Herrera, R., Barriopedro, D., 2018. Air stagnation in Europe: spatiotemporal variability and impact on air quality. Sci. Total Environ. 645, 1238–1252. https://doi.org/10.1016/j.scitotenv.2018.07.238.

Garrido-Perez, J.M., Ordóñez, C., García-Herrera, R., Schnell, J.L., 2019. The differing impact of air stagnation on summer ozone across Europe. Atmos. Environ. 219. https://doi.org/10.1016/j.atmosenv.2019.117062.

GBD 2019 Risk Factors Collaborators, 2020. Global burden of 87 risk factors in 204 countries and territories, 1990–2019: a systematic analysis for the global burden of disease study 2019. Lancet 396 (10258), 1223–1249. https://doi.org/10.1016/S0140-6736(20)30752-2.

Granier, C., Darras, S., Denier van der Gon, H., Doubalova, J., Elguindi, N., Galle, B., Gauss, M., Guevara, M., Jalkanen, J.-P., Kuenen, J., Liousse, C., Quack, B., Simpson, D., Sindelarova, K., 2019. The Copernicus Atmosphere Monitoring Service global and regional emissions (April 2019 version). In: Copernicus Atmosphere Monitoring Service (CAMS) report. https://doi.org/10.24380/d0bn-kx16.

Hersbach, H., Bell, B., Berrisford, P., Hirahara, S., Horányi, A., Muñoz-Sabater, J., Nicolas, J., Peubey, C., Radu, R., Schepers, D., Simmons, A., Soci, C., Abdalla, S., Abellan, X., Balsamo, G., Bechtold, P., Biavati, G., Bidlot, J., Bonavita, M., De Chiara, G., Dahlgren, P., Dee, D., Diamantakis, M., Dragani, R., Flemming, J., Forbes, R., Fuentes, M., Geer, A., Haimberger, L., Healy, S., Hogan, R.J., Hólm, E., Janisková, M., Keeley, S., Laloyaux, P., Lopez, P., Lupu, C., Radnoti, G., de Rosnay, P., Rozum, I., Vamborg, F., Villaume, S., Thépaut, J.N., 2020. The ERA5 global reanalysis. Q. J. Roy. Meteorol. Soc. 146. https://doi.org/10.1002/qj.3803.

Horton, D.E., Skinner, C.B., Singh, D., Diffenbaugh, N.S., 2014. Occurrence and persistence of future atmospheric stagnation events. Nat. Clim. Chang. 4 (8), 698–703. https://doi.org/10.1038/nclimate2272.

Inness, A., Ades, M., Agustí-Panareda, A., Barr, J., Benedictow, A., Blechschmidt, A.M., Jose Dominguez, J., Engelen, R., Eskes, H., Flemming, J., Huijnen, V., Jones, L., Kipling, Z., Massart, S., Parrington, M., Peuch, V.H., Razinger, M., Remy, S., Schulz, M., Suttie, M., 2019. The CAMS reanalysis of atmospheric composition. Atmos. Chem. Phys. 19, 3515–3556. https://doi.org/10.5194/acp-19-3515-2019.

Jacob, D.J., Winner, D.A., 2009. Effect of climate change on air quality. Atmos. Environ. 43, 51–63. https://doi.org/10.1016/j.atmosenv.2008.09.051.

Jenkin, M.E., Davies, T.J., Stedman, J.R., 2002. The origin and day-of-week dependence of photochemical ozone episodes in the UK. Atmos. Environ. 36 (6), 999–1012. https://doi.org/10.1016/S1352-2310(01)00360-0.

Jones, D., Prates, L., Qu, Z., Cheng, W., Miyazaki, K., Sekiya, T., Inness, A., Kumar, R., Tang, X., Worden, H., Koren, G., Huijen, V., 2025. Assessment of regional and interannual variations in tropospheric ozone in chemical reanalyses. EGUsphere. https://doi.org/10.5194/egusphere-2024-3759 preprint.

Kaiser, J.W., Heil, A., Andreae, M.O., Benedetti, A., Chubarova, N., Jones, L., Morcrette, J.J., Razinger, M., Schultz, M.G., Suttie, M., van der Werf, G.R., 2012. Biomass burning emissions estimated with a global fire assimilation system based on observed fire radiative power. J. Geophys. Res. G: Biogeosciences 9 (1), 527–554.

Konovalov, I.B., Beekmann, M., Kuznetsova, I.N., Yurova, A., Zvyagintsev, A.M., 2011. Atmospheric impacts of the 2010 Russian wildfires: integrating modelling and measurements of an extreme air pollution episode in the Moscow region. Atmos. Chem. Phys. 11, 10031–10056. https://doi.org/10.5194/acp-11-10031-2011.

Lee, J.D., Lewis, A.C., Monks, P.S., Jacob, M., Hamilton, J.F., Hopkins, J.R., Watson, N. M., Saxton, J.E., Ennis, C., Carpenter, L.J., Carslaw, N., Fleming, Z., Bandy, B.J., Oram, D.E., Penkett, S.A., Slemr, J., Norton, E., Rickard, A.R., Whalley, L.K., Heard, D.E., Bloss, W.J., Gravestock, T., Smith, S.C., Stanto, J., Pilling, M.J., Jenkin, M.E., 2006. Ozone photochemistry and elevated isoprene during the UK heatwave of august 2003. Atmos. Environ. 40 (39), 7598–7613. https://doi.org/10.1016/j.atmosenv.2006.06.057.

Li, H., Vulova, S., Rocha, A.D., Kleinschmit, B., 2024. Spatio-temporal feature attribution of European summer wildfires with Explainable Artificial Intelligence (XAI). Sci. Total Environ. 916. https://doi.org/10.1016/j.scitotenv.2024.170330.

Liu, Z., Doherty, R.M., Wild, O., O'Connor, F.M., Turnock, S.T., 2022. Tropospheric ozone changes and ozone sensitivity from the present day to the future under shared socio-economic pathways. Atmos. Chem. Phys. 22 (2), 1209–1227. https://doi.org/10.5194/acp-22-1209-2022.

Lupaşcu, A., Otero, N., Minkos, A., Butler, T., 2022. Attribution of surface ozone to NO_x and volatile organic compound sources during two different high ozone events. Atmos. Chem. Phys. 22 (17), 11675–11699. https://doi.org/10.5194/acp-22-11675-2022.

Lyapina, O., Schultz, M.G., Hense, A., 2016. Cluster analysis of European surface ozone observations for evaluation of MACC reanalysis data. Atmos. Chem. Phys. 16 (11), 6863–6881. https://doi.org/10.5194/acp-16-6863-2016.

Monks, P.S., Archibald, A.T., Colette, A., Cooper, O., Coyle, M., Derwent, R., Fowler, D., Granier, C., Law, K.S., Mills, G.E., Stevenson, D.S., Tarasova, O., Thouret, V., von Schneidemesser, E., Sommariva, R., Wild, O., Williams, M.L., 2015. Tropospheric ozone and its precursors from the urban to the global scale from air quality to short-lived climate forcer. Atmos. Chem. Phys. 15 (15), 8889–8973. https://doi.org/10.5194/acp-15-8889-2015.

Ochoa, C., Bar-Massada, A., Chuvieco, E., 2024. A European-scale analysis reveals the complex roles of anthropogenic and climatic factors in driving the initiation of large wildfires. Sci. Total Environ. 917, 170443. https://doi.org/10.1016/j.scitotenv.2024.170443.

Ordóñez, C., Barriopedro, D., García-Herrera, R., Sousa, P.M., Schnell, J.L., 2017. Regional responses of surface ozone in Europe to the location of high-latitude blocks and subtropical ridges. Atmos. Chem. Phys. 17 (4), 3111–3131. https://doi.org/10.5194/acp-17-3111-2017.

Otero, N., Sillmann, J., Schnell, J.L., Rust, H.W., Butler, T., 2016. Synoptic and meteorological drivers of extreme ozone concentrations over Europe. Environ. Res. Lett. 11, 024005. https://doi.org/10.1088/1748-9326/11/2/024005.

Otero, N., Jurado, O.E., Butler, T., Rust, H.W., 2022. The impact of atmospheric blocking on the compounding effect of ozone pollution and temperature: a copula-based approach. Atmos. Chem. Phys. 22 (3), 1905–1919. https://doi.org/10.5194/acp-22-1905-2022.

Péré, J.C., Bessagnet, B., Pont, V., Mallet, M., Minvielle, F., 2015. Influence of the aerosol solar extinction on photochemistry during the 2010 Russian wildfires episode. Atmos. Chem. Phys. 15, 10983–10998. https://doi.org/10.5194/acp-15-10983-2015.

Pope, R.J., Butt, E.W., Chipperfield, M.P., Doherty, R.M., Fenech, S., Schmidt, A., Arnold, S.R., Savage, N.H., 2016. The impact of synoptic weather on UK surface ozone and implications for premature mortality. Environ. Res. Lett. 11, 124004. https://doi.org/10.1088/1748-9326/11/12/124004.

Romero-Alvarez, J., Lupaşcu, A., Dorling, S., Reeves, C.E., Butler, T., 2025. Investigating ozone build-up in the east of England during the July 2015 heat wave. Sci. Total Environ. 979, 179464. https://doi.org/10.1016/j.scitotenv.2025.179464.

Scherrer, S.C., Croci-Maspoli, M., Schwierz, C., Appenzeller, C., 2006. Two-dimensional indices of atmospheric blocking and their statistical relationship with winter climate patterns in the Euro-Atlantic region. Int. J. Climatol. 26, 233–249. https://doi.org/10.1002/joc.1250.

Schnell, J.L., Holmes, C.D., Jangam, A., Prather, M.J., 2014. Skill in forecasting extreme ozone pollution episodes with a global atmospheric chemistry model. Atmos. Chem. Phys. 14, 7721–7739. https://doi.org/10.5194/acp-14-7721-2014.

Schnell, J.L., Prather, M.J., Josse, B., Naik, V., Horowitz, L.W., Cameron-Smith, P., Bergmann, D., Zeng, G., Plummer, D.A., Sudo, K., Nagashima, T., Shindell, D.T., Faluvegi, G., Strode, S.A., 2015. Use of North American and European air quality networks to evaluate global chemistry–climate modeling of surface ozone. Atmos. Chem. Phys. 15, 10581–10596. https://doi.org/10.5194/acp-15-10581-2015.

Sekiya, T., Emili, E., Miyazaki, K., Inness, A., Qu, Z., Pierce, R.B., Jones, D., Worden, H., Cheng, W.Y.Y., Huijnen, V., Koren, G., 2025. Assessing the relative impacts of satellite ozone and its precursor observations to improve global tropospheric ozone analysis using multiple chemical reanalysis systems. Atmos. Chem. Phys. 25 (4), 2243–2268. https://doi.org/10.5194/acp-25-2243-2025.

Seo, J., Youn, D., Kim, J.Y., Lee, H., 2014. Extensive spatiotemporal analyses of surface ozone and related meteorological variables in South Korea for the period 1999–2010. Atmos. Chem. Phys. 14 (12), 6395–6415. https://doi.org/10.5194/acp-14-6395-2014.

Soleimanian, E., Wang, Y., Li, W., Liu, X., Griggs, T., Flynn, J., Walter, P.J., Estes, M.J., 2023. Understanding ozone episodes during the TRACER-AQ campaign in Houston, Texas: the role of transport and ozone production sensitivity to precursors. Sci. Total Environ. 900, 165881. https://doi.org/10.1016/j.scitotenv.2023.165881.

Sousa, P.M., Trigo, R.M., Barriopedro, D., Soares, P.M.M., Ramos, A.M., Liberato, M.L.R., 2017. Responses of European precipitation distributions and regimes to different blocking locations. Climate Dynam. 48, 1141–1160. https://doi.org/10.1007/s00382-016-3132-5.

Sousa, P.M., Trigo, R.M., Barriopedro, D., Soares, P.M.M., Santos, J.A., 2018. European temperature responses to blocking and ridge regional patterns. Climate Dynam. 50, 457–477. https://doi.org/10.1007/s00382-017-3620-2.

Sousa, P.M., Barriopedro, D., García-Herrera, R., Woollings, T., Trigo, R.M., 2021. A new combined detection algorithm for blocking and subtropical ridges. J. Climate 34 (18), 7735–7758. https://doi.org/10.1175/JCLI-D-20-0658.1.

Turnock, S.T., Allen, R., Archibald, A.T., Dalvi, M., Folberth, G., Griffiths, P.T., Keeble, J., Robertson, E., O'Connor, F.M., 2022. The future climate and air quality response from different near-term climate forcer, climate, and land-use scenarios using UKESM1. Earth's Future 10 (8), e2022EF002687. https://doi.org/10.1029/2022EF002687.

Vieno, M., Dore, A.J., Stevenson, D.S., Doherty, R., Heal, M.R., Reis, S., Hallsworth, S., Tarrason, L., Wind, P., Fowler, D., Simpson, D., Sutton, M.A., 2010. Modelling surface ozone during the 2003 heat-wave in the UK. Atmos. Chem. Phys. 10 (16), 7963–7978. https://doi.org/10.5194/acp-10-7963-2010.

Zanis, P., Hadjinicolaou, P., Pozzer, A., Tyrlis, E., Dafka, S., Mihalopoulos, N., Lelieveld, J., 2014. Summertime free-tropospheric ozone pool over the eastern Mediterranean/Middle East. Atmos. Chem. Phys. 14 (1), 115–132. https://doi.org/10.5194/acp-14-115-2014.

Ziv, B., Saaroni, H., Alpert, P., 2004. The factors governing the summer regime of the eastern Mediterranean. Int. J. Climatol. 24, 1859–1871. https://doi.org/10.1002/joc.1113.